

pubs.acs.org/Macromolecules Article

Synthesis and Characterization of Amine-Epoxy-Functionalized Polystyrene-block-Poly(glycidyl methacrylate) to Manage Morphology and Covarying Properties for Self-Assembly

Hongbo Feng, Chang-Geun Chae, Christopher Eom, Gordon S. W. Craig, Stuart J. Rowan,* and Paul F. Nealey*



Cite This: Macromolecules 2023, 56, 2675-2685



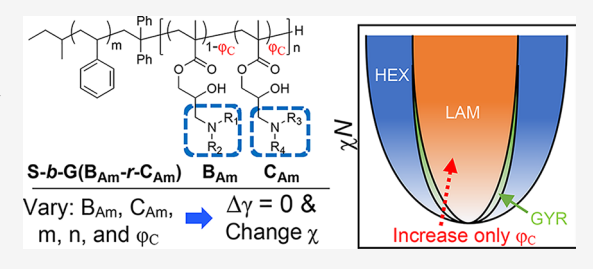
ACCESS I

III Metrics & More

Article Recommendations

Supporting Information

ABSTRACT: "Click" chemistry modification of a block copolymer to generate A-b-(B-r-C) block-random copolymers (BRCs) has been proven as an effective method to manage covarying properties of a block copolymer, such as the effective interaction parameter (χ_{eff}) and the surface energy difference of the two blocks ($\Delta \gamma$). Reported herein is a study of the modification of the glycidyl methacrylate block of polystyrene-blockpoly(glycidyl methacrylate) (S-b-G) with amine-epoxy "click" chemistry. Three pairs of more polar and less polar secondary amines are selected to modify S-b-G to make a series of lamellae-forming BRCs to determine what



ratio of the more polar amine in the random block ($\varphi_{\rm C}$) is necessary to achieve $\Delta \gamma = 0$. The dependence of the $\chi_{\rm eff}$ of each BRC on $\varphi_{\rm C}$ is determined from SAXS measurements. For advanced lithography applications, a lamellae-forming BRC with sub-10 nm features and $\Delta \gamma = 0$ is demonstrated. Utilizing the $\chi_{\rm eff} - \phi_{\rm C}$ relationship, a set of BRCs are synthesized from a single S-b-G such that amine-epoxy modification generates disordered, cylindrical, gyroidal, and lamellar morphologies, depending on $\varphi_{\mathbb{C}}$.

INTRODUCTION

Block-random copolymers (BRCs), which are block copolymers (BCPs) in which at least one of the blocks is a random copolymer, provide the opportunity to leverage the benefits of BCP systems, such as their amphiphilic nature, diverse functionality, and microphase morphology, while simultaneously providing a method to manage multiple, potentially orthogonal properties by controlling the relative amounts of the different monomers in the random copolymer block. Applications of BRCs range from car tires² to marine antifouling and fouling release coatings.³ The thermodynamics of a BRC is more complicated than a linear A-b-B BCP because of the presence of binary interactions, which are strongly associated with the chemical components and their molar ratios. In a simple case, the thermodynamics of BRCs with an A-b-(B-r-C) architecture is governed by three pairwise interactions (A-B, A-C, and B-C) and the molar ratio of C in the B-r-C block $(\phi_{\rm C})^4$ In one example of the thermodynamic complexity of a BRC, Wei et al. synthesized poly(ethylene oxide)-block-poly(n-butyl methacrylate-randompropargyl methacrylate) as an A-b-(B-r-C) BRC that underwent a disorder-to-order transition upon an alkyne-azide "click" reaction of the propargyl methacrylate group with azide-functionalized rhodamine B.5 In a demonstration of BRCs relevant to advanced lithography, which requires the formation of perpendicularly orientated domains preferably via thermal annealing with a free surface, Kim et al. used A-b-(B-r-C) BRCs formed by the partial epoxidation of polyisoprene in

polystyrene-block-polyisoprene (S-b-I) with isoprene and epoxidized isoprene as the B and C components, respectively. With the appropriate molar ratio of isoprene (less polar than S) and epoxidized isoprene (more polar than S), the surface energy (γ) of the S block could be balanced by the γ of the partially epoxidized I block, such that the difference of γ of the two blocks $(\Delta \gamma)$ equaled zero, enabling the formation of perpendicular domains at the free surface by thermal annealing. This approach also enabled decoupling of the effective Flory-Huggins interaction parameter (χ_{eff}) from $\Delta \gamma$. In a similar approach with polystyrene-block-polybutadiene (S-b-B), thiolene "click" chemistry was used to bond a variety of chemical groups to the butadiene units, creating a random block of butadiene and thiol-modified butadiene. As such, a variety of C components of the A-b-(B-r-C) components could be formed, providing this system with more flexibility than that was possible partially epoxidized S-b-I. Both perpendicular cylindrical and lamellar morphologies were obtained from the resulting BRCs. More recently, this approach was extended with a series of BRCs developed from thiol-epoxy "click"

Received: December 20, 2022 Revised: March 7, 2023 Published: March 28, 2023





chemistry modification of polystyrene-block-poly(glycidyl methacrylate) (S-b-G). The epoxy units were reacted to completion with a combination of two thiols to create the B and C parts of an A-b-(B-r-C) BRC. The ability to modify poly(glycidyl methacrylate) (G) with a pair of thiols with different polarity and at different molar ratios of the more polar component (φ_C) provided a powerful platform to generate a range of BRCs with different lamellar spacings but with $\Delta \gamma = 0$. Additionally, formation of the BRCs with two different components, as opposed to partial functionalization with just one component as in the cases above, offered an immense array of alternatives.

Amine-epoxy "click" chemistry and S-b-G provide another route to expand the BRC platform. Similar to the thiol-epoxy case, the amine-epoxy reaction enables the attachment to G of a wide variety of chemical moieties, such as hydroxy groups using 2-(methylamino)ethanol (MOH) and Si-containing components using N-(trimethylsilylmethyl)benzylamine (BnTMS). By modifying G with a pair of amines with different polarities, such as MOH and BnTMS, the final amine-functionalized G block can have the same γ as the S block. Unlike the thiol-ene or thiol-epoxy reactions, the amineepoxy reaction does not require any external agent such as 2,2'azobis(2-methylpropionitrile) (used in thiol-ene chemistry) or lithium hydroxide catalyst (used in thiol-epoxy chemistry). Importantly, the amine-epoxy product does not leave sulfur in the final BRC, which may be undesirable in some semiconductor manufacturing applications.

In this work, amine-epoxy "click" chemistry is used with a parent S-b-G to explore the effects that the amine group size and functionality have on the resulting BRC in terms of χ_{eff} and morphology. The γ of G reacted to completion with each of six different amines is measured to find amine pairs that result in the modified G having a γ either lower or higher than the γ of S; G modified with those amines are denoted as G(B_{Am}) and $G(C_{Am})$. Then, three candidate pairs of B_{Am} and C_{Am} amines are selected for morphological studies: BnTMS and MOH, BnTMS and 2-(2-methylaminoethyl)pyridine (MPy), and Nmethylpropylamine (MPr) and MOH. For each B_{Am} and C_{Am} pair, a series of BRCs with different φ_C are synthesized, with $\varphi_{\rm C}$ determined from ¹H NMR spectroscopy. Small-angle X-ray scattering (SAXS) is used to analyze the morphology and domain spacing of the modified BRC S-b-G(BAm-r-CAm) as a function of ϕ_{C} . The χ_{eff} values of these BRCs are then estimated using their domain spacings. Utilizing the $\chi_{\rm eff}$ – $\phi_{\rm C}$ relationship, a new S-b-G with a slightly higher volume fraction of S (f_S) is functionalized. The resulting collection of BRCs generates a range of morphologies, including the Ia3d gyroids morphology. Evaluation of χ_{eff} and f_{S} of each BRC reveals that in many cases for these BRCs, morphological transitions in the phase diagram are accessed more by changes in $\chi_{\rm eff}$ than in $f_{\rm S}$. Additionally, a lamellae-forming BRC with sub-10 nm features and $\Delta \gamma = 0$ is demonstrated.

MATERIALS AND METHODS

Materials. Styrene (St, 99%, Aldrich), glycidyl methacrylate (GMA, 99%, Aldrich), sec-butyllithium (sec-BuLi, 1.4 M, Aldrich), 1,1-diphenylethylene (DPE, 97%, Aldrich), lithium chloride (LiCl, 99.95%, Aldrich), tetrahydrofuran (THF, 99.9%, Fisher Chemical), methylcyclohexane (McHEX, 99%, Aldrich), methanol (MeOH, 99%, Fisher Chemical), N-methylpropylamine (MPr, 96%, Aldrich), N-methylethanolamine (MOH, 98%, Aldrich), N-[(trimethylsilyl)methyl]benzylamine (BnTMS, 98%, Aldrich), 2-(2-methylaminoethyl)pyridine (MPy, 97%, Aldrich), N-(2-

methoxyethyl)methylamine (MMeO, 97%, Aldrich), N-methyl-2-phenylethylamine (MPh, 99%, Aldrich), diethanolamine (diOH, 98%, Aldrich), N-M-dimethylformamide (DMF, anhydrous, 99.8%, Aldrich), acetonitrile (99.9%, Fisher Scientific), toluene (99.8%, Fisher Scientific), ethanol (anhydrous, 99.5%, Fisher Scientific), propylene glycol methyl ether acetate (PGMEA, 99.5%, Aldrich), and diiodomethane (CH $_2$ I $_2$, 99%, Aldrich) were used without further purification unless otherwise noted. Inhibitor included with commercially purchased St and GMA was removed prior to use. Dimethyl sulfoxide- d_6 with 0.03 vol % tetramethylsilane (DMSO- d_6 , 99.9 atom% D, Aldrich) and chloroform-d with 0.03 vol % tetramethylsilane (CDCl $_3$, 99.8 atom% D, Aldrich) were used as received.

Anionic Polymerization of Poly(Glycidyl Methacrylate) (G) and Polystyrene-Block-Poly(Glycidyl Methacrylate) (S-b-G). Homopolymer G and BCP S-b-G were synthesized via living anionic polymerization and Schlenk techniques. The detailed synthetic procedure can be found in the literature.8 An example synthesis of S-b-G is described below. To a five-neck anionic reactor was added McHEX (60 mL) followed by St (11.6 mL, 100.8 mmol). A gas-tight syringe was used to add 1.2 mL of sec-BuLi solution (1.4 M) to the reaction mixture. The color of the mixture turned from colorless to orange, a characteristic color of the living anionic polymerization of S. The reaction mixture was stirred for 4 h at 40 °C. An aliquot of living S solution was taken using a gas-tight syringe and precipitated into degassed MeOH. The obtained homopolymer S was characterized by size exclusion chromatography (SEC) to obtain the number-averaged molecular weight (M_n) and dispersity (D) of the first block. To the mixture was added 2 mL of DPE (4 equiv) and the mixture was stirred for 15 min. The reactor was then slowly cooled to -78 °C followed by the addition of THF (250 mL) and LiCl (712 mg, 10 equiv) and stirred for an extra 5 min to ensure thermal equilibration. The mixture was stirred for another 30 min. The desired amount of GMA (11.1 mL, 4.23 M, 47.1 mmol in one example) in THF was then added to the mixture and stirred for another 30 min. Upon the addition of GMA monomers, the color of the solution turned from dark red to colorless. After 30 min, to the reaction mixture was added degassed methanol (3 mL), which terminated polymerization. The reaction mixture was then warmed to room temperature, concentrated, precipitated from hexanes twice, and dried in a vacuum oven at 40 °C. The purified product was obtained as a white powder and characterized using ¹H NMR and SEC.

S of
$$S_{87}$$
-b- G_{38} : SEC $-M_n = 9.1 \text{ kg mol}^{-1}$, $D = 1.02$

S of
$$S_{75}$$
-b- G_{42} : SEC $-M_n = 7.9 \text{ kg mol}^{-1}$, $D = 1.01$

S-b-G: ^{1}H NMR (CDCl $_{3}$ with 0.03 vol % TMS, 400 MHz): δ (ppm), 7.23–6.25 (br), 4.39–4.23 (br), 3.88–3.73 (br), 3.29–3.19 (br), 2.90–2.79 (br), 2.69–2.59 (br), 2.29–1.67 (br), 1.67–1.20 (br), 1.20–1.00 (br), 0.99–0.51 (br).

$$S_{87}$$
-b- G_{38} : SEC - $M_n = 14.7 \text{ kg mol}^{-1}$, $D = 1.06$

$$S_{75}$$
-b- G_{42} : SEC - $M_n = 14.1 \text{ kg mol}^{-1}$, $D = 1.04$

An example synthesis of G homopolymer is described as follows. To a five-neck anionic reactor equipped with a glass-coated stir bar was added LiCl (415 mg, 10 equiv, pre-vacuum dried) and 0.70 mL of DPE (2.83 M, 4 equiv). The reactor was then slowly cooled to -78 °C followed by the addition of 0.70 mL of *sec*-BuLi solution (1.4 M) and stirred for an extra 30 min. The color of the reaction mixture turned from colorless to dark red upon addition of *sec*-BuLi. In one example, the desired amount of GMA (7.0 mL, 4.23 M, 42.2 mmol) in THF was then added to the mixture and stirred for another 30 min. Upon the addition of GMA, the color of the solution turned from dark red to colorless. After 30 min, to the reaction mixture was added degassed methanol (3 mL), which terminated the polymerization. The reaction mixture was then warmed to room temperature, concentrated, precipitated from hexanes twice, and dried in a vacuum oven at 40 °C. The purified product was obtained as a white powder.

G: $^1{\rm H}$ NMR (CDCl $_3$ with 0.03 vol % TMS, 400 MHz): δ (ppm), 4.39–4.23 (br), 3.88–3.73 (br), 3.29–3.19 (br), 2.90–2.79 (br), 2.69–2.59 (br), 2.14–1.82 (br), 1.19–0.51 (br). SEC: $M_{\rm n}$ = 8.3 kg mol $^{-1}$, D = 1.03.

General Synthetic Procedure for Monoamine-Functionalized G Homopolymers (G(Amine)). A 40 mL cylindrical vial was charged with a magnetic stirrer, G (100 mg), a solvent (4 mL of acetonitrile for nonpolar amine or a 1:1 (v/v) mixture of acetonitrileethanol for polar amine), and a secondary amine (10 molar equiv. to the epoxide rings). The reaction mixture was stirred at 80 °C. A few aliquots were extracted at 24 h intervals for ¹H NMR until it was confirmed that the epoxy groups were no longer present in the sample and that G had reacted to completion. After the reaction was complete, acetonitrile was removed under reduced pressure and the remaining part was dissolved in a minimal amount of a good solvent for the polymer (THF for nonpolar amines and DMF for polar amines). The resulting polymer was isolated from the residual amine by precipitation in a poor solvent (hexanes for nonpolar amines and diethyl ether for polar amines), centrifugation, and removal of the liquid. The above isolation cycle was repeated three times in total. Finally, the G(Amine) homopolymer was transferred into a vial and dried under vacuum to yield a pure product.

G(BnTMS): ¹H NMR (CDCl₃ with 0.03 vol % TMS, 400 MHz): δ (ppm) 7.35–7.00 (br), 4.10–3.80 (br), 3.80–3.45 (br), 3.45–3.25 (br), 2.55–1.50 (br), 1.10–0.60 (br), 0.15–0 (br).

G(MPr): ^1H NMR (DMSO- d_6 with 0.03 vol % TMS, 400 MHz): δ (ppm) 7.30–7.00 (br), 4.90–4.55 (br), 4.05–3.85 (br), 3.85–3.60 (br), 2.40–2.23 (br), 2.23–2.10 (br), 2.05–1.55 (br), 1.50–1.30 (br), 1.10–0.60 (br).

G(MPh): ¹H NMR (DMSO- d_6 with 0.03 vol % TMS, 400 MHz): δ (ppm) 7.35–7.00 (br), 4.80–4.55 (br), 4.05–3.85 (br), 3.85–3.60 (br), 2.70–2.60 (br), 2.60–2.45 (br), 2.45–2.27 (br), 2.27–2.10 (br), 2.10–1.55 (br), 1.10–0.60 (br).

G(MMeO): ¹H NMR (DMSO- d_6 with 0.03 vol % TMS, 400 MHz): δ (ppm) 7.30–7.00 (br), 4.80–4.60 (br), 4.05–3.85 (br), 3.85–3.60 (br), 3.45–3.35 (br), 3.25–3.15 (br), 2.60–2.50 (br), 2.45–2.30 (br), 2.30–2.20 (br), 2.10–1.50 (br), 1.10–0.60 (br).

G(MPy): ^1H NMR (DMSO- 4 6 with 0.03 vol % TMS, 400 MHz): δ (ppm) 8.45–8.35 (br), 7.70–7.55 (br), 7.25–7.17 (br), 7.17–7.00 (br), 4.95–4.75 (br), 4.00–3.55 (br), 2.90–2.75 (br), 2.75–2.60 (br), 2.45–2.27 (br), 2.27–2.10 (br), 2.10–1.50 (br), 1.10–0.60 (br).

G(MOH): 1 H NMR (DMSO- d_{6} with 0.03 vol % TMS, 400 MHz): δ (ppm) 7.30–7.00 (br), 4.85–4.65 (br), 4.50–4.30 (br), 4.05–3.85 (br), 3.85–3.60 (br), 3.55–3.40 (br), 2.49–2.43 (br), 2.43–2.30 (br), 2.30–2.15 (br), 2.10–1.50 (br), 1.10–0.60 (br).

G(diOH): ¹H NMR (DMSO- d_6 with 0.03 vol % TMS, 400 MHz): δ (ppm) 7.30–7.00 (br), 4.85–4.60 (br), 4.55–4.30 (br), 4.05–3.85 (br), 3.85–3.60 (br), 3.50–3.35 (br), 2.70–2.40 (br), 2.10–1.50 (br), 1.10–0.60 (br).

General Synthetic Procedure for Monoamine-Functionalized S-b-G (S-b-G(Amine)). A 40 mL cylindrical vial was charged with a magnetic stirrer, S-b-G (100 mg), a solvent (4 mL of 1:1 (v/v)mixture of toluene and acetonitrile for BnTMS, MPr, MPh, MMeO, and MPy; 6 mL of 1:1:1 (v/v/v) mixture of toluene, acetonitrile, and ethanol for MOH and diOH), and the amine (10 molar equiv. to the epoxide rings). The reaction mixture was stirred at 80 °C. A few aliquots were extracted at 24 h intervals for ¹H NMR and SEC analyses until it was confirmed that the epoxide rings in G were completely consumed. Then, the solvents were evaporated under reduced pressure and the remaining material was dissolved in a minimal amount of a good solvent (THF for nonpolar-aminefunctionalized S-*b*-G and DMF for polar-amine-functionalized S-*b*-G). The resulting polymer was then isolated from residual amine through precipitation into a poor solvent (hexanes for nonpolar amines and diethyl ether for polar amines), centrifugation, and removal of the liquid. The above isolation cycle was repeated three times in total. Finally, the monoamine-functionalized S-b-G (S-b-G(Amine)) polymer was transferred into a vial and dried under vacuum to yield a pure product.

S-*b*-G(BnTMS): ¹H NMR (CDCl₃ with 0.03 vol % TMS, 400 MHz): δ (ppm) 7.40–7.18 (br), 7.18–6.85 (br), 6.75–6.30 (br), 4.10–3.80 (br), 3.80–3.45 (br), 3.45–3.25 (br), 2.55–1.25 (br), 1.10–0.60 (br), 0.15–0 (br).

S-*b*-G(MPr): ¹H NMR (CDCl₃ with 0.03 vol % TMS, 400 MHz): δ (ppm) 7.25–6.85 (br), 6.75–6.30 (br), 4.15–3.70 (br), 2.50–2.30 (br), 2.30–2.15 (br), 2.10–1.20 (br), 1.20–0.75 (br).

S-*b*-G(MPh): ¹H NMR (CDCl₃ with 0.03 vol % TMS, 400 MHz): δ (ppm) 7.40–6.85 (br), 6.75–6.30 (br), 4.10–3.60 (br), 2.85–2.55 (br), 2.50–2.20 (br), 2.10–1.20 (br), 1.20–0.75 (br).

S-b-G(MMeO): 1 H NMR (CDCl $_{3}$ with 0.03 vol % TMS, 400 MHz): δ (ppm) 7.25–6.85 (br), 6.75–6.30 (br), 4.15–3.70 (br), 3.55–3.40 (br), 3.40–3.25 (br), 2.80–2.55 (br), 2.55–2.40 (br), 2.40–2.25 (br), 2.10–1.20 (br), 1.20–0.75 (br).

S-b-G(MPy): ¹H NMR (CDCl₃ with 0.03 vol % TMS, 400 MHz): δ (ppm) 8.55–8.45 (br), 7.65–7.50 (br), 7.25–6.85 (br), 6.75–6.30 (br), 4.60–4.30 (br), 4.10–3.75 (br), 3.00–2.70 (br), 2.55–2.35 (br), 2.35–2.20 (br), 2.10–1.20 (br), 1.20–0.75 (br).

S-b-G(MOH): ¹H NMR (DMSO- d_6 with 0.03 vol % TMS, 400 MHz): δ (ppm) 7.30–6.85 (br), 6.75–6.25 (br), 4.85–4.65 (br), 4.50–4.30 (br), 4.05–3.85 (br), 3.85–3.60 (br), 3.55–3.40 (br), 2.49–2.43 (br), 2.43–2.30 (br), 2.30–2.15 (br), 2.10–1.20 (br), 1.10–0.60 (br).

S-b-G(diOH): ¹H NMR (DMSO- d_6 with 0.03 vol % TMS, 400 MHz): δ (ppm) 7.30–6.85 (br), 6.75–6.25 (br), 4.85–4.60 (br), 4.55–4.30 (br), 4.05–3.85 (br), 3.85–3.60 (br), 3.50–3.35 (br), 2.70–2.40 (br), 2.10–1.20 (br), 1.10–0.60 (br).

General Synthetic Procedure for Amine-Functionalized S-b-**G BRCs** (S- \dot{b} -G(B_{Am}-r-C_{Am})). The synthetic procedure for S-b-G(B_{Am}-r-C_{Am}) generally followed the synthetic procedure for S-b-G(Amine) described above. A 40 mL cylindrical vial was charged with a magnetic stirrer, S-b-G (100 mg), a solvent (4 mL of 1:1 (v/v) mixture of toluene and acetonitrile for BnTMS, MPr, MPh, MMeO, and MPy; 6 mL of 1:1:1 (v/v/v) mixture of toluene, acetonitrile, and ethanol for MOH and diOH), and the two amines (total 10 molar equiv. to the epoxide rings). The molar ratio of the two amines in the feed was recorded. The reaction mixture was stirred for 48 h at 80 °C. The conversion was monitored by extracting aliquots at 24 h intervals for ¹H NMR and SEC analyses until it was confirmed that the epoxide rings in G were completely consumed. Then, the solvents were evaporated under reduced pressure and the remaining material was dissolved in a minimal amount of a good solvent (THF for nonpolaramine-functionalized S-b-G and DMF for polar-amine-functionalized S-b-G). The desired product was purified using the same techniques described previously. 1 H NMR was used to determine $\varphi_{\rm C}$ in the final product. $\varphi_{\rm C}$ was then compared with the molar ratios of the two amines in the feed. This relationship provided critical guidance in the synthesis to achieve a desired $\varphi_{\rm C}$.

Material Characterization. SEC was performed on a Shimadzu gel permeation chromatography system equipped with a Wyatt DAWN HELEOS II multi-angle light scattering detector, a Wyatt ViscoStar III differential viscometer, a Wyatt Optilab T-rEX differential refractive index detector, and a Shimadzu SPD-M₃₀A photodiode array detector (200-800 nm). THF was used as the eluent and the column sets were 2 Agilent PLgel 5 μ m MIXED-D plus guard. The D and M_n values of G and S-b-G were determined using multi-angle laser light scattering detectors (the dn/dc of G is 0.0931 mL g^{-1} , the dn/dc of S is 0.185 mL g^{-1} , and the dn/dc of S-b-G was calculated following the literature⁸). ¹H NMR was performed with a Bruker AVANCE III HD NanoBay 400 MHz. Scanning electron microscopy (SEM) images were captured on a Zeiss Merlin highresolution field-emission SEM instrument with a 1-2 keV accelerating voltage at a working distance below 4 mm using the inlens secondary electron detector. Image brightness and contrast were adjusted for presentation. Atomic force microscopy (AFM) was performed on a Bruker Nanoscope IIIa Multimode 5 atomic force microscope in standard tapping mode.

Small-Angle X-ray Scattering. SAXS data were collected on a SAXSLAB (XENOCS)'s GANESHA system. An X-ray beam with $\lambda = 0.154$ nm was used. A Pilatus 300 K solid state photon-counting

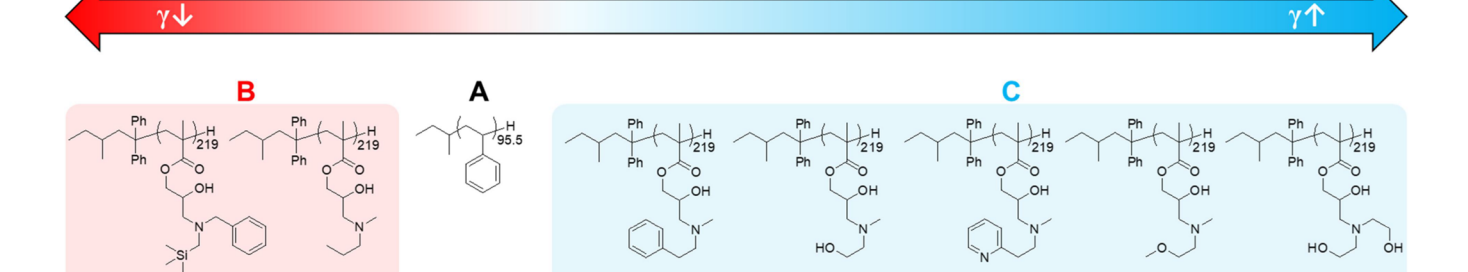


Figure 1. Surface energy (γ) of polystyrene (S) and seven homopolymers of poly(glycidyl methacrylate) (G) monofunctionalized with different amines (G(Amine)). Different γ values identify G(Amine) homopolymers that are less polar (B) and more polar(C) than S to make an A-b-(B-r-C) block-random copolymer with blocks that have equal γ .

G(MOH):

 $50.9 \pm 1.1 \; mN \; m^{-1}$

G(MPh):

 $47.1 \pm 0.7 \; mN \; m^{-1}$

detector was used. The exposure time was 1200 s to obtain a good signal-to-noise ratio. Before measurement, the samples for room temperature SAXS were annealed in a vacuum chamber at 150 °C for 20 h. SAXSGUI software was used for data reduction from a 2D image data to a 1D profile. The domain periodicity, L_0 , of the BRCs and BCPs was calculated using $L_0 = 2\pi/q^*$, where q^* is the Bragg principal peak of the SAXS scan.

 $44.2 \pm 0.6 \; mN \; m^{-1}$

G(MPr):

 $40.9 \pm 1.6 \; mN \; m^{\text{-}1}$

G(BnTMS):

 $38.3 \pm 0.9 \text{ mN m}^{-1}$

Effective Flory–Huggins Interaction Parameter ($\chi_{\rm eff}$) Calculation. $\chi_{\rm eff}$ was determined using an equation developed for the strong segregation regime (SSR), $^{8,1.2}$

$$L_0 = 1.10aN^{2/3} \chi_{\text{eff}}^{1/6} \tag{1}$$

where a is the statistical segment chain length and N is the number of statistical segments normalized to a reference volume of 144 ų. The BRCs in this work are not in the SSR, but previous research showed that eq 1 provides a reasonable estimate even when $\chi N < 20$, ¹³ and as shown below, the $\chi_{\rm eff}$ estimates were used only in terms of a comparison to other estimates of $\chi_{\rm eff}$ in this work. The statistical segment chain length of each BRC ($a_{\text{S-b-G(BAm-r-CAm)}}$) was calculated with the following equation:

$$a_{S-b-G(B_{Am}-r-C_{Am})} = \frac{1}{\sqrt{\frac{f_S}{a_S^2} + \frac{f_{G(B_{Am}-r-C_{Am})}}{a_{G(B_{Am}-r-C_{Am})}^2}}}}$$
(2)

where f_S and $f_{G(BAm-r-CAm)}$ are the respective volume fractions of the two blocks, and a_S is the statistical segment chain length of S, 0.68 nm. $a_{G(BAm-r-CAm)}$ is assumed to be close to the statistical segment chain length of G, 0.65 nm. ^{13,14} The N of S_m -b- $G(B_{Am}$ -r- $C_{Am})_n$ is calculated with the following equation:

$$\begin{split} N &= N_{\rm S} + N_{\rm G(B_{Am}-r-C_{Am})} \\ &= \frac{1}{144} \frac{1}{N_{\rm A}} \left(\frac{m \cdot {\rm MW_{St}}}{\rho_{\rm S}} \right. \\ &+ \frac{n \cdot {\rm MW_{GMA}} + n(1 - \varphi_{\rm C}) \cdot {\rm MW_{B_{Am}}} + n \varphi_{\rm C} \cdot {\rm MW_{C_{Am}}}}{\rho_{\rm G(B_{Am}-r-C_{Am})}} \right) \end{split}$$

where $N_{\rm A}$ is Avogadro's constant, m and n are determined from the $M_{\rm n}$ of S_m and S_m -b- G_m respectively, and $MW_{\rm St}$ and $MW_{\rm GMA}$ are the molar mass of St and GMA monomer, respectively. $MW_{\rm BAm}$ and $MW_{\rm CAm}$ are the molar mass of $B_{\rm Am}$ and $C_{\rm Am}$, respectively. The density (ρ) values of the different $G(B_{\rm Am}$ -r- $C_{\rm Am})$ random blocks are calculated using the molar ratio of $B_{\rm Am}$ and $C_{\rm Am}$ and the densities $\rho_{G(B_{\rm Am})}$ and $\rho_{G(C_{\rm Am})}$, which are determined from Parachor parameters. ^{15,16} The corresponding ρ values are shown in Table S1. ρ_S is the density of S, 1.04 g cm⁻³.

Metrology. Film thicknesses were measured using a J.A. Woollam Alpha SE ellipsometer. A Si-SiO_x-Cauchy model was used to obtain

the thickness where the native oxide SiO_x layer was preset at 1.5 nm. For films under 10 nm, the optical constants were first fit to thick films and then locked to capture the film thickness more accurately.

G(MMeO):

 $54.5\pm1.2~mN~m^{\text{-}1}$

G(diOH):

58.2 ± 1.8 mN m

G(MPy):

 $54.2 \pm 2.5 \; mN \; m^{-1}$

Island-Hole Test. Solutions of S-b-G(B_{Am} -r-C $_{Am}$) (0.3 wt % in THF) were spin-coated onto silicon wafers freshly cleaned with piranha solution (caution: piranha solution is highly corrosive and reacts violently with organic matter!), yielding films with thicknesses of $1.67L_0$ - $1.76L_0$. The thin films were then annealed at 150 °C for 30 min in vacuum and characterized by AFM and SEM. A detailed interpretation of the island-hole test can be found in the literature. ¹⁷

Surface Energy (γ) Measurements. A KRÜSS drop shape analyzer 100 was used to measure the γ of each G(Amine). Solutions of each G(Amine) in PGMEA or THF were spin-coated on a piranhacleaned silicon wafer to form thin films with thickness of ~30 nm. In a N₂-filled glove box, the thin films were baked on a hot plate at 150 °C for 1 h and then placed on a block of metal to cool to room temperature. Contact angles of deionized water and CH₂I₂ were measured to determine the γ of each material. Before each measurement, dry N₂ was blown over the film surface to remove particle contaminants. The contact angle was measured using the sessile drop method and the drop volume was 1 μ L for each measurement. The left and right contact angles of each drop were averaged, and 10 sessile drops were deposited for each sample. γ was then calculated using the OWRK method. ^{18,19}

Thermal Properties. Thermogravimetric analysis (TGA) was carried out in an N_2 atmosphere on a TA Instruments Discovery 5500 thermogravimetric analyzer. The samples were first equilibrated at 110 °C for 10 min to remove any attached volatiles such as trapped solvent molecules and moisture and then heated to 600 °C at a rate of $10\ ^{\circ}\text{C}$ min $^{-1}$. Differential scanning calorimetry (DSC) was carried out on a TA Instruments Discovery 2500 differential scanning calorimeter in an N_2 atmosphere. The samples were first thermally equilibrated at $120\ ^{\circ}\text{C}$ for 10 min, followed by a cooling ramp to $-80\ ^{\circ}\text{C}$ at a rate of $10\ ^{\circ}\text{C}$ min $^{-1}$ and then stabilized for 5 min. The samples were then heated back to $120\ ^{\circ}\text{C}$ at a rate of $10\ ^{\circ}\text{C}$ min $^{-1}$. The glass transition temperature was measured on the second heating cycle.

RESULTS AND DISCUSSION

To characterize the morphologies of the different BRCs in this system, it was important to select amines that could undergo the amine-epoxy reaction with G without affecting its dispersity. To limit the potential of the amines acting as cross-linking agents, secondary amines were used, as shown in Scheme S1. A variety of amines were evaluated to determine the surface energy of each G(Amine). The goal was to find pairs of amines, B_{Am} and C_{Am} , resulting in the amine-modified G random copolymer block having either a lower or higher surface energy than S. To do this, G and S homopolymers were synthesized via living anionic polymerization, as shown for G

Scheme 1. Synthesis of Parent BCP and Functionalized BRC

 a (a) The synthesis of S-*b*-G parent BCP via living anionic polymerization. (b) Thiol-amine functionalization of S-*b*-G to yield S-*b*-G(B_{Am}-*r*-C_{Am}) BRC, where B_{Am} and C_{Am} are the less and more polar secondary amines, respectively. The pairs of amines used in the work are shown in the pane at the bottom.

in Scheme S2. For the initial part of the study, seven amines were selected for evaluation, BnTMS, MOH, MPy, MPr, MMeO, MPh, and diOH. To determine suitable reaction conditions in this study, solvents, reaction time, and reaction temperature were briefly screened with G and S-b-G and the different amines. Initially, the reactions were monitored by eye to look for evidence of insolubility or cross-linking. From these initial experiments, a toluene-acetonitrile mixture (ethanol was added in the case of hydroxy containing amines) was used to minimize the formation of aggregates, especially for the modification on S-b-G. Subsequent screening tests determined that a reaction time of 48 h was sufficient to ensure full conversion of the amine-epoxy reaction at 80 °C without crosslinking, which was verified with ¹H NMR and SEC. The corresponding ¹H NMR spectra and SEC profiles of G and each G(Amine) are shown in Figures S1-S9, respectively. Then, the γ for each G(Amine) was calculated using the OWRK method and contact angle measurements with water (Figure S10) and CH_2I_2 . Using the same method, the γ of S was determined to be 44.2 ± 0.6 mN m⁻¹, which was close to the value of 42.6 mN m⁻¹ in the literature determined with the same method and liquids.²⁰ A comparison of the γ of each G(Amine) to the γ of S is presented in Figure 1. From this comparison, the following (B_{Am}, C_{Am}) pairs were selected: (BnTMS, MPy), (BnTMS, MOH), and (MPr, MOH).

The BRCs used in this work were synthesized according to Scheme 1. The parent polymer, S_m -b- G_n (the subscripts m and n represent the average number of repeat units in each block), was synthesized via living anionic polymerization with

sequential addition of the S and G monomers. The value of m was calculated from the M_n of the homopolymer S, using SEC of an aliquot of the S block taken from the anionic polymerization prior to the addition of the G monomer. With a known value of m, the n was then calculated from the ¹H NMR integral of the BCP (Figure S11). The obtained S_m -b- G_n was monofunctionalized with each of the amines to create reference ¹H NMR spectra of S-b-G(Amine) for each amine (Figures S12-S18). The corresponding SEC profiles are presented in Figure S19. Then, S_m -b- G_n was functionalized with three pairs of amines, as shown in Scheme 1b. For each pair of amines, a series of BRCs with a range of φ_C values was synthesized, where φ_C was controlled by the feed ratios of the amines and characterized using ¹H NMR integrals (Figure 2). The SEC profiles for each series in Figure S20 show that functionalization with pairs of amines at different φ_C led to shorter elution times, indicating higher M_n values than S_{87} -b-G₃₈ but no large change of the shapes of the elution peaks, indicating that amine functionalization did not lead to large changes in D.

Figure 2 shows representative 1 H NMR spectra of S-*b*-G and of three S-*b*-G(B_{Am}-*r*-C_{Am}) BRCs synthesized according to Scheme 1. The complete disappearance of the characteristic peaks of methylene protons next to the ester group, $-C(O)O-C\underline{H}_2-$, in G (peak a at 4.31 ppm in CDCl₃) indicates the full conversion of the epoxy functionality. The 1 H NMR spectra of each S-*b*-G(Amine) are shown in Supporting Information Figures S12–17. The relationship between the molar ratio of amines in the feed and the corresponding

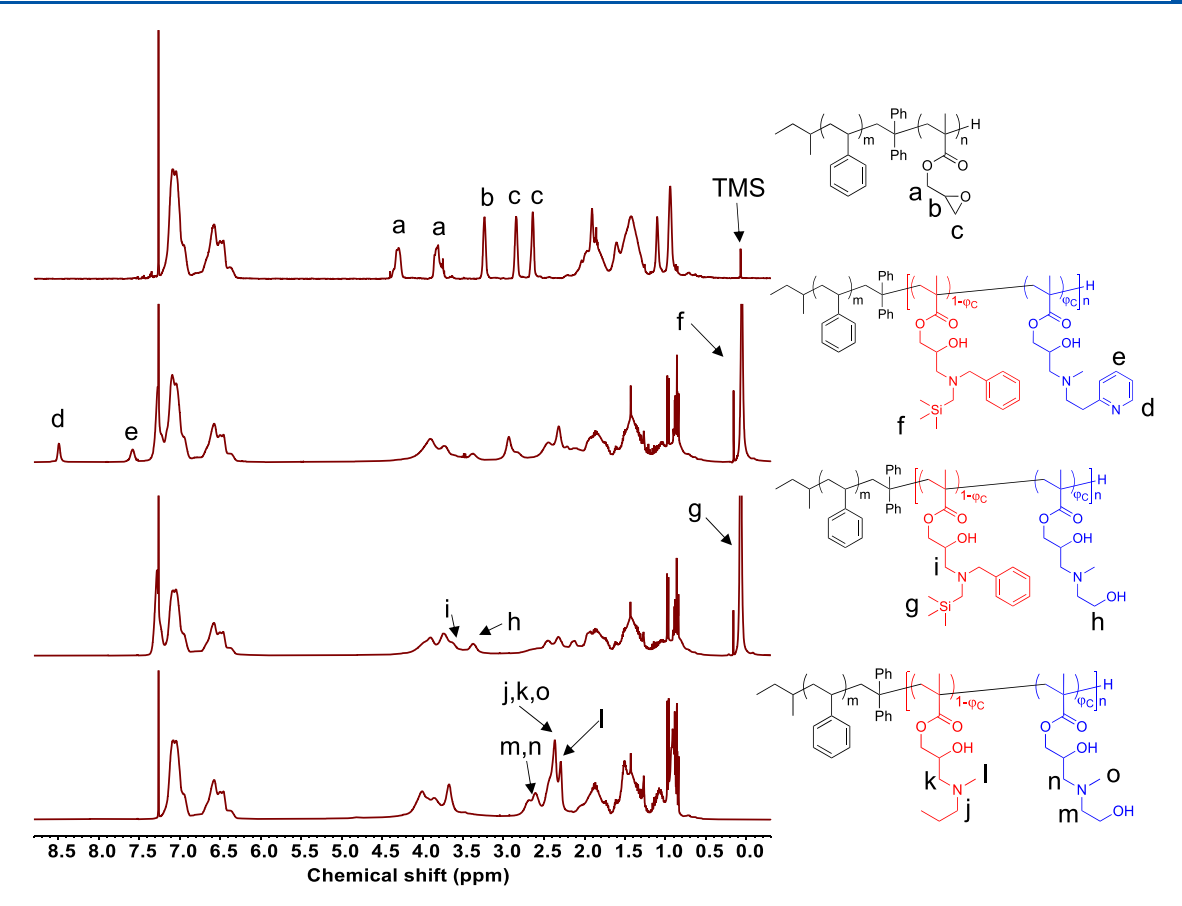


Figure 2. 1 H NMR spectra of S_{87} -b- G_{38} , S_{87} -b-G(BnTMS-r-MPy)₃₈, S_{87} -b-G(BnTMS-r-MOH)₃₈, and S_{87} -b-G(MPr-r-MOH)₃₈, synthesized according to Scheme 1b. The peak assignments in each spectrum are assigned to the hydrogen atoms identified in the polymer structure to the right of the spectrum.

measured $\varphi_{\rm C}$ of the S-b-G(B_{Am}-r-C_{Am}) BRCs is shown in Figure 3. The deviation from a 1:1 linear relationship, especially for amine pairs BnTMS/MPy and BnTMS/MOH, suggests that steric hinderance plays an important role in reaction kinetics.

Starting with a single parent BCP, S_{87} -b- G_{38} with $f_S = 0.657$, a series of S-b- $G(B_{Am}$ -r- $C_{Am})$ BRCs with different φ_C was synthesized for each of the three pairs of amines. To determine a proper annealing temperature of S-b- $G(B_{Am}$ -r- $C_{Am})$, thermal properties were characterized with TGA and DSC, as shown in Figure S21. An annealing temperature of 150 °C was selected

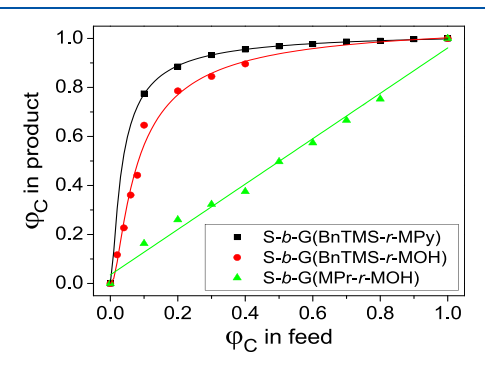


Figure 3. Epoxy-amine functionalization of S-b-G, in terms of the measured ratio of the more polar amine in the random block $(\varphi_{\mathbb{C}})$ in the block-random copolymer (BRC) as a function of $\varphi_{\mathbb{C}}$ in the feed for the three S-b-G(B_{Am}-r-C_{Am}) BRCs. The solid lines serve as a guide to the eye.

because it is higher than the glass transition temperatures of the BRCs but lower than the degradation temperature. The addition of the amines to the G block led to a decrease in $f_{\rm S}$, but only down to 0.430. As a result, all the resulting BRC morphologies were lamellar, as shown in the SAXS scans in Figure 4. For the S₈₇-b-G(BnTMS-r-MPy)₃₈ and S₈₇-b-G(BnTMS-r-MOH)₃₈ series at low $\varphi_{\rm MPy}$ and $\varphi_{\rm MOH}$, respectively, the BRCs are in the disordered state, which suggests a relatively low $\chi_{\rm eff}$ at these $\varphi_{\rm C}$ values. The S₈₇-b-G(MPr-r-MOH)₃₈ series remains in a lamellar state for all $\varphi_{\rm MOH}$ from 0 to 1. No significant even order peaks were observed at $\varphi_{\rm MOH}$ < 0.375, suggesting that $f_{\rm S}\sim$ 0.5 for these BRCs.

The $\chi_{\rm eff}$ values of the BRCs were estimated with eq 1, which is only strictly appropriate in the SSR, whereas the BRCs were not in the SSR. However, previous research showed that eq 1 provides reasonable estimates even for $\chi N < 20^{.6,13}$ More importantly, the calculated values of $\chi_{\rm eff}$ were internally consistent and thus allowed for direct comparison of the BRCs in this work. The $\chi_{\rm eff}$ values of these A-b-(B-r-C)-type BRCs followed a quadratic relationship with respect to $\varphi_{\rm C}$ because of the A-B, A-C, and B-C binary interactions, with corresponding interaction parameters $\chi_{\rm A-b-B}$, $\chi_{\rm A-b-C}$, and $\chi_{\rm B-b-C}$.

$$\chi_{\text{eff,A-}b-(B-r-C)} = \chi_{B-b-C} \varphi_{C}^{2} + (\chi_{A-b-C} - \chi_{A-b-B} - \chi_{B-b-C}) \varphi_{C} + \chi_{A-b-B}$$

$$(4)$$

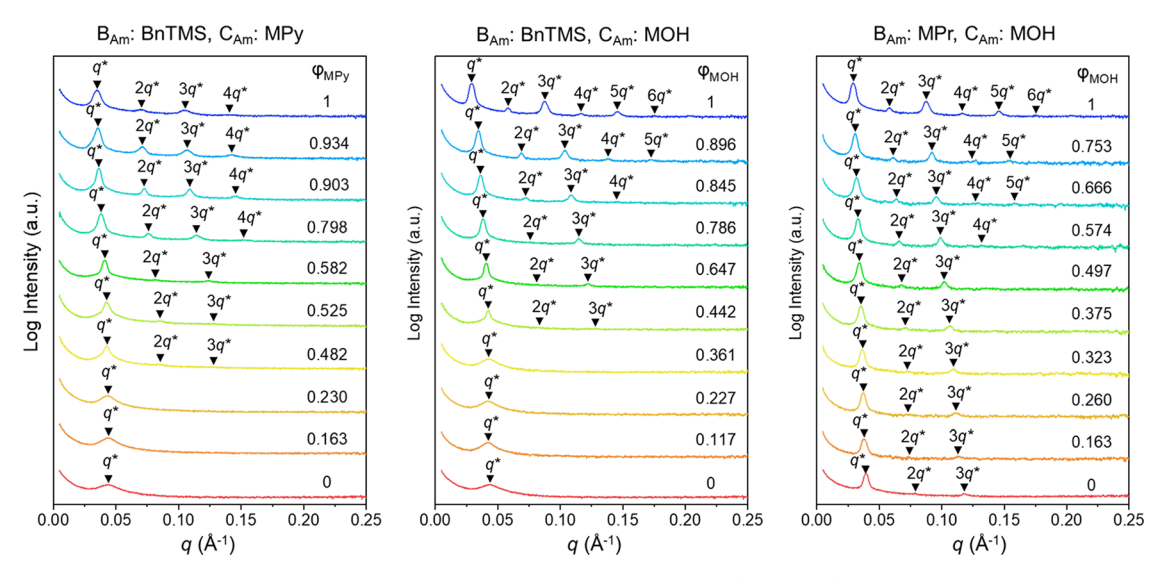


Figure 4. Bulk transmission SAXS profiles of three different amine-functionalized S_{87} -b- $G(B_{Am}$ -r- $C_{Am})_{38}$. Lines are shifted vertically for clarity. The degree of functionalization of the polar C amine (φ_C) in each BCP is labeled.

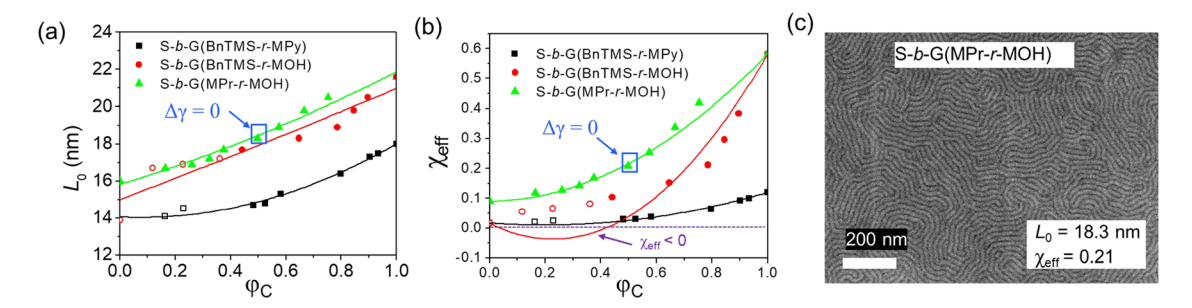


Figure 5. (a) Domain periodicity (L_0) as a function of φ_C for three BRCs. The lines represent a second-order polynomial fitting. Open symbols indicate that the BRCs are in a disordered state, and their values are included in the fitting for consistency. (b) Plot of $\chi_{\rm eff}$ as a function of φ_C for the three BRCs. $\chi_{\rm eff}$ values of the BRCs in the disordered state, open symbols, are not included for the second-order polynomial fitting. From the fitting, the $\chi_{\rm eff}$ of S_{87} -b-G(BnTMS-r-MOH)₃₈ at a small range of φ is less than 0, indicative of favored mixing. The purple dashed line represents $\chi_{\rm eff} = 0$. In both plots, the blue box around a data point indicates the φ_C value for S_{87} -b-G(MPr-r-MOH)₃₈ at which the surface energy (γ) of the S and the G(MPr-r-MOH) blocks are equal, and $\Delta \gamma = 0$. (c) Top-down SEM image of a self-assembled thin film of S_{87} -b-G(MPr-r-MOH)₃₈ at the $\varphi_C = 0.497$ value identified in (a) and (b).

Table 1. Summarized Quadratic Function Fit Parameters and χ Values of the Three Pairwise Interactions of A-B, A-C, and B-C for each of the A-B-(B-r-C) BRCs that Were Studied

BRC	χ_{A-b-B}	χ_{A-b-C}	χ_{B-b-C}	best fit quadratic function ^a	R^2
S_{87} -b-G(BnTMS-r-MPy) ₃₈	0.0164	0.120	0.170	$\chi_{\text{eff}} = 0.170 \varphi_{\text{C}}^2 - 0.0667 \varphi_{\text{C}} + 0.0164$	0.9831
S_{87} -b-G(BnTMS-r-MOH) ₃₈	0.0164	0.582	1.038	$\chi_{\text{eff}} = 1.0385 \varphi_{\text{C}}^2 - 0.4732 \varphi_{\text{C}} + 0.0164$	0.8700
S_{87} - b - $G(MPr$ - r - $MOH)_{38}$	0.0893	0.582	0.436	$\chi_{\rm eff} = 0.436 \varphi_{\rm C}^2 + 0.0559 \varphi_{\rm C} + 0.0893$	0.9892

^aThe function fit was for the three sets of data was performed to simultaneously maximize the R^2 values using Microsoft Excel 16.69 Solver, and the fit functions were forced to pass through the data points at $\varphi_C = 0$ and 1. The data points where the BRCs were in the disordered state were not included in the fitting.

The effect of $\varphi_{\rm C}$ on L_0 , and the corresponding $\chi_{\rm eff}$ of the three BRCs in Figure 2 is shown in Figure 5a,b. The calculated $\chi_{\rm eff}$ values of the three BRCs as a function of $\varphi_{\rm C}$ were fit well by a quadratic function, as predicted by eq 4. As shown in previous work with BRCs, ^{6–8} values of $\varphi_{\rm C}$ could be found at which $\Delta \gamma = 0$, and at those values, self-assembly of a thin film of the BRC resulted in a fingerprint structure of lamellar domains, as shown in Figure 5c. The values of $M_{\rm n}$, $f_{\rm S}$, $\chi_{\rm eff}$ and $\chi_{\rm eff}N$ for each of the BRCs with $\Delta \gamma = 0$ are presented in Table S2.

The three sets of χ_{eff} data shown in Figure 5b are fit simultaneously with eq 4 because $\chi_{\text{S-b-G(BnTMS)}}$ and $\chi_{\text{S-b-G(MOH)}}$

appear twice in the three fitting equations. Additionally, because the BnTMS-modified BRCs at low $\varphi_{\rm C}$ were in the disordered state, as shown in Figure 4, and the $\chi_{\rm eff}$ values estimated at low $\varphi_{\rm C}$ are inherently suspect. Thus, these $\chi_{\rm eff}$ values were not included in the fit, except for the value at $\varphi_{\rm C}=0$, which was included to guarantee that the $\chi_{\rm S-b-G(BnTMS)}$ value corresponded to the disordered state. Second, for all three BRCs, the fitting function was constrained to include the $\chi_{\rm eff}$ value determined at $\varphi_{\rm C}=0$ and 1. The fitting parameters, corresponding to $\chi_{\rm A-b-B}$, $\chi_{\rm A-b-C}$, and $\chi_{\rm B-b-C}$ values and fit quality (R^2), are presented in Table 1. The R^2 value for each BRC was generally good. The R^2 value for S₈₇-b-G(BnTMS-r-MOH)₃₈

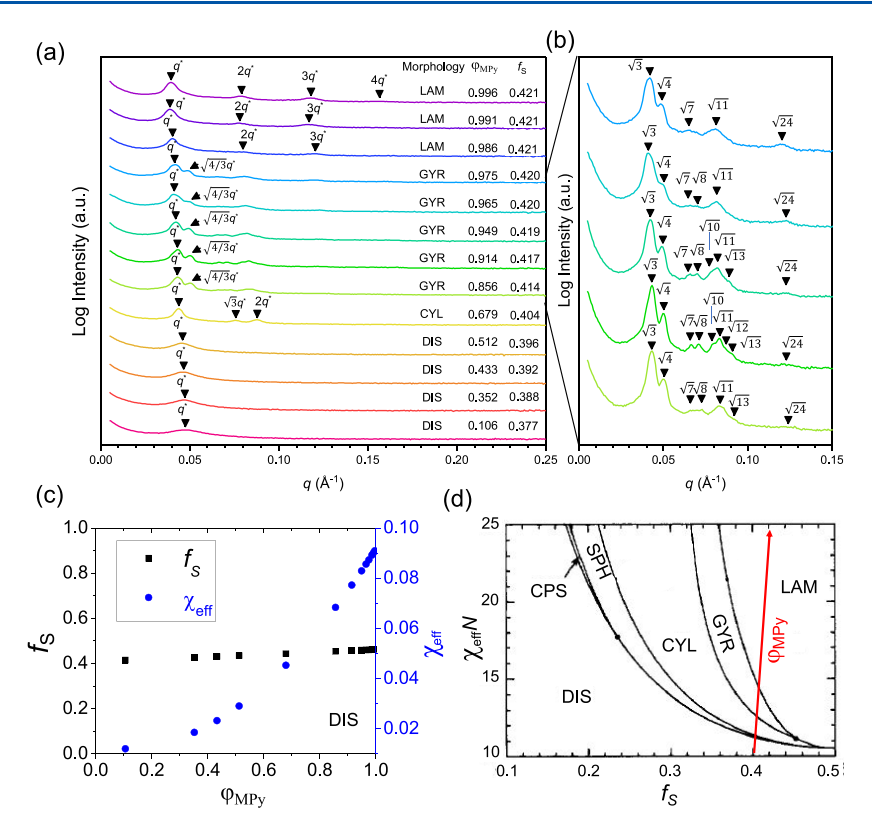


Figure 6. Effect of φ_{MPy} on the χ_{eff} and morphology of S_{75} -b-G(BnTMS-r-MPy)₄₂ block-random copolymer. (a) SAXS scans of S_{75} -b-G(BnTMS-r-MPy)₄₂ at φ_{MPy} ranging from 0.996 to 0.106. The morphology, φ_{MPy} , and volume fraction of S (f_S) at each composition ratio are labeled. LAM, lamellae; GYR, $Ia\overline{3}d$ gyroids; CYL, hexagonally close-packed cylinders; DIS, disordered. (b) Enlargement of SAXS scans from $Ia\overline{3}d$ GYR-forming S_{75} -b-G(BnTMS-r-MPy)₄₂ with detailed peak assignment. (c) Plots of f_S (left y axis) and χ_{eff} (right y axis) as a function of φ_{MPy} , where the χ_{eff} is calculated using quadratic fit function of entry 1 in Table 1. (d) A phase diagram based on mean field theory from ref 35 illustrating the morphology evolution as a function of f_S . As φ_{MPy} increases, f_S increases from 0.377 to 0.421 while $\chi_{eff}N$ increases more significantly from 2.6 to 24.5, as indicated by the red arrow in the diagram.

was slightly lower, presumably because there were fewer eligible data points for use in the fit.

The fits to eq 4 provide an opportunity to estimate χ_{B-b-C} without synthesizing the corresponding B-b-C BCP. It is important to note that the values for χ_{B-b-C} reported here are only estimations as the BRCs are not in the SSR. Additionally, it is assumed that $a_{G(B_{Am}-r-C_{Am})}$ and a_{G} are the same and that the density of G(B_{Am}-r-C_{Am}), which is essential for calculating N, f, and $a_{S-b-G(BAm-r-CAm)}$, is the same for all of the amines, which is likely not accurate. However, while the χ_{B-b-C} values estimated in this work are not intended to be used as definitive values, they can be useful for internal comparisons of the different chemistries. Using the assumptions outlined above, the $\chi_{\text{B-}b\text{-}C}$ interaction parameters are determined to be 0.170 $(\chi_{G(BnTMS)-b-G(MPy)})$, 1.038 $(\chi_{G(BnTMS)-b-G(MOH)})$, and 0.436 $(\chi_{G(MPr)-b-G(MOH)})$. χ_{B-b-C} is generally larger than χ_{A-b-C} and χ_{A-b-B} because of the larger difference of polarity between B and C than between A and C or A and B. In the extreme, the fit suggests that over a small range of $\varphi_{\rm C}$ (0–0.3), the $\chi_{\rm eff}$ of S₈₇-b- $G(BnTMS-r-MOH)_{38}$ is less than that of S_{87} -b- $G(BnTMS-r-MOH)_{38}$ MPy)₃₈, as shown in Figure 5b. In an even narrower $\varphi_{\rm C}$ window (0.1–0.2), $\chi_{\text{eff S-}b\text{-}G(BnTMS-}r\text{-}MOH)}$ < 0, indicative of favored mixing. This could be possible because BnTMS and MOH had the largest χ_{B-b-C} . The energy penalty of MOH interacting with BnTMS could cause the MOH lattice sites to be closer to the S lattice sites despite being part of the random block, resulting in a negative χ_{eff} . Such an interaction is analogous to the improved miscibility between S and natural

rubber (polyisoprene) with partial epoxidation.21 However, unlike the thioether moiety that is present when the thiolepoxy click reaction is used to generate BRCs from S-b-G, the amine moiety in this work can serve as a good hydrogen bond acceptor, and in some cases, hydrogen bonds can provide enough of an enthalpic gain to overcome polarity differences between chemical moieties and therefore lower their χ value. For example, $\chi_{\text{B-}b\text{-C}}$ in S_{87} -b-G(MPr-r-MOH)₃₈ is smaller than χ_{A-b-C} , which is possibly a result of hydrogen bonding interactions between the relatively nonpolar G(MPr) and the relatively polar G(MOH). The effect of hydrogen bonding on χ has been previously reported, such as in the case of a polymer blend consisting of poly(4-vinyl pyridine) and poly(4-hydroxystyrene), which had a smaller χ than a blend containing less polar poly(2-vinylpyridine) and poly(4hydroxystyrene) as a result of the hydroxy group having stronger H-bonding interactions with 4-vinylpyridine than with 2-vinylpyridine.^{22,23} The effect of hydrogen bonding in this analysis suggests that in developing BCPs, simply connecting blocks with large differences in polarity does not necessarily lead to BCPs with high χ values.

One of the desirable attributes of BCPs, including BRCs, for use in directed self-assembly (DSA) for advanced lithographic patterning is that they have $\Delta \gamma = 0$ such that thermal annealing results in BCP domains perpendicular to the free surface. Early studies on DSA predominantly used polystyrene-block-poly-(methyl methacrylate) (S-b-M), 25,26 which has $\Delta \gamma = 0$ at annealing temperatures but also has a low χ value such that its

lowest attainable L_0 is ~22 nm. ²⁷ Zhou et al. maintained the $\Delta \gamma = 0$ of S-b-M by adding vinylnapthalene to the S block, making a BRC with a higher $\chi_{\rm eff}$ than S-b-M. ²⁸ Seshimo et al. achieved a high χ and $\Delta \gamma = 0$ with a BCP containing S by modifying the other block, a polysiloxane, with hydroxyl groups. ²⁹ Yoshimura et al. made an A-b-B diblock BCP with $\Delta \gamma = 0$ by modifying S-b-G with a single thiol that contained two different chemical moieties that were selected to increase χ while balancing the γ of the two blocks. ³⁰ However, in their approach, they could not vary the ratio of the two chemical moieties, as can be done in the work presented here. Yoshida et al. have demonstrated a BRC with $\Delta \gamma = 0$ that was derived by post-processing S-b-M with an ester—amide exchange reaction such that a small number of the M repeat units were converted into methacrylamides. ³¹

While each of the above methods for achieving a higher χ than S-b-M while maintaining $\Delta \gamma = 0$ is impressive, there are limitations in terms of the breadth of BCPs that can be generated with a desired $\chi_{\rm eff}$ value and $\Delta \gamma = 0$. The approach taken here follows the method previously reported for the functionalization of S-b-G with thiol-epoxy click chemistry to rapidly access a variety of BRCs with different χ values while still having $\Delta \gamma = 0.8$ As the method uses two different molecules to functionalize one of the blocks to make a BRC, a systematic approach can be used to quickly find a BRC with $\Delta \gamma = 0$. As such, a series of S₈₇-b-G(MPr-r-MOH)₃₈ BRCs were made with different $\varphi_{\rm C}$ values, and then, island-hole tests were performed to determine φ_C that resulted in $\Delta \gamma = 0$. The island-hole test results are presented in Figure S22. As $\varphi_{\rm C}$ increased from 0.260 to 0.753, a topographic transition from $1L_0$ islands to a $0.5L_0$ flat film and then to $1L_0$ holes was observed. The $0.5L_0$ topographic feature was observed, which indicated that $\Delta \gamma = 0$, at $\varphi_{\rm C} = 0.497$. As shown in the SEM image in Figure 5c, self-assembly of S₈₇-b-G(MPr-r-MOH)₃₈ with $\Delta \gamma = 0$ resulted in the expected fingerprint morphology with 9 nm lines and spaces. Ostensibly, this material could undergo DSA on a chemical pattern, as demonstrated in previous work with BRCs. 7,8

The ability to access nanostructures with different geometries, especially the ones beyond lamellae, is essential to expand the array of applications of BRCs. 7,32,33 Interestingly, we found that changing $\varphi_{\rm C}$ with the amine-epoxy click chemistry enabled us to explore the different morphologies in the BCP phase diagram by changing $\chi_{\rm eff}$ while making only minor changes in f_S . Leveraging the capability of changing $\chi_{\rm eff}$ using BRCs, the capability of obtaining other morphologies by changing $\varphi_{\rm C}$ was explored. First, a new S₇₅-b-G₄₂ with a higher $f_S = 0.572$ than the previous S_{87} -b- G_{38} was synthesized such that the f_S values after functionalization would be in the range of 0.38-0.42 and thus offer access to a variety of morphologies. S₇₅-b-G₄₂ was reacted with BnTMS and MPy in different combinations to achieve a range of ϕ_{MPy} values. DSC was performed on the resulting S₇₅-b-G(BnTMS-r-MPy)₄₂ BRCs to verify that they could be annealed at 150 °C (Figure S23). Then, SAXS was performed on the different BRCs to determine the effect of φ_{MPy} on morphology (Figure 6a). As φ_{MPv} increased from 0 to 1, the morphology transitioned from disordered to hexagonally close-packed cylinders to Ia3d gyroids and finally to lamellae. A detailed peak assignment of the SAXS scans of the BRCs with the $Ia\overline{3}d$ gyroidal morphology is shown in Figure 6b. $^{34}\chi_{\rm eff}$ for this series of S₇₅-b-G(BnTMS-r-MPy)₄₂ was then calculated by using the φ_{MPv} value with the quadratic fit function in Table 1 for the

corresponding amine pair. The plots of $f_{\rm S}$ and $\chi_{\rm eff}$ as a function of φ_{MPy} , shown in Figure 6c, reveal that the change in χ_{eff} was more significant than the change in f_S after amine functionalization. In particular, as $\phi_{ ext{MPy}}$ increased the $\chi_{ ext{eff}}N$ of S_{75} -b-G(BnTMS-r-MPy)₄₂ increased from 2.6 to 24.5 (an 840% increase) while the f_S increased from 0.377 to 0.421 (a 12% increase). In Figure 6d, the effect of the increase in φ_{MPv} on f_S and $\chi_{\text{eff}}N$ is shown schematically as a red arrow overlaid on a previously reported theoretical BCP phase diagram.³⁵ Only the red trend arrow is shown in Figure 6d, and not the individual $(f_S, \chi_{eff}N)$ data, because previous work has shown that while experimental phase diagrams qualitatively match the theoretical phase diagram, there are notable quantitative differences. The $f_{\rm S}$ and $\chi_{\rm eff}N$ values are summarized in Table S3. Thus, this high-throughput platform combining amine-epoxy click chemistry and S-b-G enabled us to explore the different morphologies in the BCP phase diagram while making only minor changes in f_S .

Extensive research has been performed to access different BCP morphologies and to compare theoretically predicted phase diagrams, such as the one shown in Figure 6d, with experimental results. For example, Winey et al. made a series of S-b-I BCPs near the order-disorder transition (ODT) with f_S ranging from 0.21 to 0.76, from which they outlined a phase diagram.³⁷ Khandpur et al. constructed an improved phase diagram based on ten separate S-b-I BCPs near the ODT with $f_{\rm S}$ ranging from 0.18 to 0.76.³⁸ In these cases, χN was held relatively constant (near the ODT), and the different morphologies were probed by varying f_S . In contrast, with one S-b-I BCP, and therefore constant f_S , Sakurai et al. thermoreversibly accessed cylindrical and spherical morphologies by heating the material to change $\chi^{.39}$ As mentioned above, Wei et al. used an alkyne-azide "click" reaction to increase γ and go from the disordered to the ordered regime of the BCP phase diagram. Subsequently, they tuned the volume fraction of their PEO block and the alkyne/azide ratio in their system, akin to $f_{\rm S}$ and $\varphi_{\rm C}$ in the work reported here, and showed with the appropriate starting BCP that they could generate either lamellar or cylindrical morphologies, depending on the alkyne/azide ratio. 40 The work here also uses click chemistry to access different morphologies in the phase diagram, but it differs in that reaction to completion of one of the blocks with two different amines provides a much broader array of possibilities in terms of attainable chemistries and their corresponding χ values.

CONCLUSIONS

The amine-epoxy click reaction was used to modify S-b-G to yield a series of S-b-G(B_{Am}-r-C_{Am}) BRCs with A-b-(B-r-C) architecture, decoupling the thermodynamics and surface energies. For advanced lithography, a lamellae-forming S-b-G(MPr-r-MOH) with sub-10 nm feature size and perpendicular orientation attainable via industry-preferred thermal annealing with a free surface was demonstrated. $\chi_{\rm eff}$ parameters at each $\varphi_{\rm C}$ were determined using strong-segregation theory. In addition, χ values of the three pairwise interactions of A-B, A-C, and B-C for each of the A-b-(B-r-C) BRCs were revealed using a binary interaction model. Because of the unique second-order dependence of $\chi_{\rm eff}$ on $\varphi_{\rm C}$, the use of different amine pairs with the appropriate parent BCP enabled the formation of a range of morphologies, including gyroids, hexagonally close-packed cylinders, and lamellae. This work shows a promising approach that offers access to a wide range

of morphologies in the BCP phase diagram without the complicated iterative synthesis commonly done in the past. This along with machine learning and predictive models further paves the way for structure—property studies using BRCs. Importantly, this work demonstrates a new high-throughput chemistry platform in which key parameters of the materials required for patterning applications including χ , γ , and f_S can be independently modulated.

ASSOCIATED CONTENT

Supporting Information

The Supporting Information is available free of charge at https://pubs.acs.org/doi/10.1021/acs.macromol.2c02552.

Amine-epoxy reaction of primary and secondary amines with G; 1H NMR spectra of G homopolymer, G functionalized with the seven amines used in the study, S-b-G, and the seven corresponding S-b-G(Amine) BCPs; SEC profiles of G, the G(Amine) homopolymers, S-b-G, S-b-G(Amine) BCPs, and the three S-b-G(B_{Am}-r-C_{Am}) BRCs in the study; water contact angle measurements of the G(Amine) homopolymers; thermogravimetric and DSC analysis profiles of S, G, and the G(Amine) homopolymers; island-hole tests on S-b-G(MPr-r-MOH) at different values of φ_{MOH} ; DSC profiles of S₇₅-b-G(BnTMS-r-MPy)₄₂; Parachor-determined density values of G and G(Amine) homopolymers; characterization values of the amine-functionalized S-b-G BRCs; morphology and calculated χ_{eff} $\chi_{\text{eff}}N$, and f_S of S_{75} -b-G(BnTMS-r-MPy)₄₂ at different values of φ_{MPv} (PDF).

AUTHOR INFORMATION

Corresponding Authors

Stuart J. Rowan — Pritzker School of Molecular Engineering, University of Chicago, Chicago, Illinois 60637, United States; Department of Chemistry, University of Chicago, Chicago, Illinois 60637, United States; orcid.org/0000-0001-8176-0594; Email: stuartrowan@uchicago.edu

Paul F. Nealey — Pritzker School of Molecular Engineering, University of Chicago, Chicago, Illinois 60637, United States; orcid.org/0000-0003-3889-142X; Email: nealey@uchicago.edu

Authors

Hongbo Feng — Pritzker School of Molecular Engineering, University of Chicago, Chicago, Illinois 60637, United States; orcid.org/0000-0002-8806-6041

Chang-Geun Chae – Korea Research Institute of Chemical Technology, Daejeon 34114, Republic of Korea;
orcid.org/0000-0001-8805-6743

Christopher Eom — Pritzker School of Molecular Engineering, University of Chicago, Chicago, Illinois 60637, United States

Gordon S. W. Craig — Pritzker School of Molecular Engineering, University of Chicago, Chicago, Illinois 60637, United States; Oorcid.org/0000-0002-0224-3511

Complete contact information is available at: https://pubs.acs.org/10.1021/acs.macromol.2c02552

Author Contributions

H.F. and C.-G.C. contributed equally to this work.

The authors declare no competing financial interest.

ACKNOWLEDGMENTS

This research was supported by the U.S. Department of Commerce, National Institute of Standards and Technology, as part of the Center for Hierarchical Materials Design (CHiMaD). This work made use of the shared facilities at the University of Chicago Materials Research Science and Engineering Center, supported by National Science Foundation under award number DMR-2011854. It also made use of the Pritzker Nanofabrication Facility of the Pritzker School of Molecular Engineering at the University of Chicago, which receives support from Soft and Hybrid Nanotechnology Experimental (SHyNE) Resource (NSF ECCS-1542205), a node of the National Science Foundation's National Nanotechnology Coordinated Infrastructure. Part of this work was carried out at the Soft Matter Characterization Facility of the University of Chicago.

REFERENCES

- (1) Tsitsilianis, C.; Gotzamanis, G.; Iatridi, Z. Design of "Smart" Segmented Polymers by Incorporating Random Copolymers as Building Blocks. *Eur. Polym. J.* **2011**, *47*, 497.
- (2) Jangareddy, S.; Register, R. A. Incorporation of Styrene into a Model Polyolefin for Enhanced Compatibility with Polyisoprene. *Macromolecules* **2020**, *53*, 9142.
- (3) Patterson, A. L.; Wenning, B.; Rizis, G.; Calabrese, D. R.; Finlay, J. A.; Franco, S. C.; Zuckermann, R. N.; Clare, A. S.; Kramer, E. J.; Ober, C. K.; Segalman, R. A. Role of Backbone Chemistry and Monomer Sequence in Amphiphilic Oligopeptide- and Oligopeptoid-Functionalized PDMS- and PEO-Based Block Copolymers for Marine Antifouling and Fouling Release Coatings. *Macromolecules* **2017**, *50*, 2656
- (4) Paul, D. R.; Barlow, J. W. A Binary Interaction-Model for Miscibility of Copolymers in Blends. *Polymer* 1984, 25, 487.
- (5) Wei, X. Y.; Chen, W.; Chen, X. J.; Russell, T. P. Disorder-to-Order Transition of Diblock Copolymers Induced by Alkyne/Azide Click Chemistry. *Macromolecules* **2010**, *43*, 6234–6236.
- (6) Kim, S.; Nealey, P. F.; Bates, F. S. Decoupling Bulk Thermodynamics and Wetting Characteristics of Block Copolymer Thin Films. ACS Macro Lett. 2012, 1, 11.
- (7) Feng, H.; Dolejsi, M.; Zhu, N.; Griffin, P. J.; Craig, G. S. W.; Chen, W.; Rowan, S. J.; Nealey, P. F. Synthesis and Characterization of Block Copolymers for Nanolithography Based on Thiol-Ene "Click" Functionalized Polystyrene-Block-Polybutadiene. *Adv. Funct. Mater.* **2022**, 32, No. 2206836.
- (8) Feng, H.; Dolejsi, M.; Zhu, N.; Yim, S.; Loo, W.; Ma, P.; Zhou, C.; Craig, G. S. W.; Chen, W.; Wan, L.; Ruiz, R.; de Pablo, J. J.; Rowan, S. J.; Nealey, P. F. Optimized Design of Block Copolymers with Covarying Properties for Nanolithograpy. *Nat. Mater.* **2022**, *21*, 1426–1433.
- (9) Feng, H.; Lu, X. Y.; Wang, W. Y.; Kang, N. G.; Mays, J. W. Block Copolymers: Synthesis, Self-Assembly, and Applications. *Polymer* **2017**, *9*, 494.
- (10) Geng, Z. S.; Shin, J. J.; Xi, Y. M.; Hawker, C. J. Click Chemistry Strategies for the Accelerated Synthesis of Functional Macromolecules. *J. Polym. Sci.* **2021**, *59*, 963–1042.
- (11) Ehlers, J.-E.; Rondan, N. G.; Huynh, L. K.; Pham, H.; Marks, M.; Truong, T. N. Theoretical Study on Mechanisms of the Epoxy–Amine Curing Reaction. *Macromolecules* **2007**, *40*, 4370.
- (12) Semenov, A. N. Contribution to the Theory of Microphase Layering in Block-Copolymer Melts. Zh. Eksp. Teor. Fiz. 1985, 88, 1242.
- (13) Ren, Y.; Lodge, T. P.; Hillmyer, M. A. Synthesis, Characterization, and Interaction Strengths of Difluorocarbene-Modified Polystyrene-Polyisoprene Block Copolymers. *Macromolecules* **2000**, 33, 866.

Macromolecules Article pubs.acs.org/Macromolecules

- (14) Zdyrko, B.; Klep, V.; Luzinov, I. Synthesis and Surface Morphology of High-Density Poly(ethylene glycol) Grafted Layers. Langmuir 2003, 19, 10179.
- (15) Sewell, J. H. Method of Calculating Densities of Polymers. J. Appl. Polym. Sci. 1973, 17, 1741-1747.
- (16) Loo, W. S.; Feng, H.; Ferron, T. J.; Ruiz, R.; Sunday, D. F.; Nealey, P. F. Determining Structure and Thermodynamics of A-b-(Br-C) Copolymers. ACS Macro Lett. 2023, 12, 118.
- (17) Maher, M. J.; Bates, C. M.; Blachut, G.; Sirard, S.; Self, J. L.; Carlson, M. C.; Dean, L. M.; Cushen, J. D.; Durand, W. J.; Hayes, C. O.; Ellison, C. J.; Willson, C. G. Interfacial Design for Block Copolymer Thin Films. Chem. Mater. 2014, 26, 1471.
- (18) Kaelble, D. H. Dispersion-Polar Surface Tension Properties of Organic Solids. J. Adhes. 1970, 2, 66.
- (19) Owens, D. K.; Wendt, R. C. Estimation of Surface Free Energy of Polymers. J. Appl. Polym. Sci. 1969, 13, 1741-1747.
- (20) Wu, S. Calcluation of Interfacial Tension in Polymer Systems. J. Polym. Sci., C Polym. Symp. 1971, 34, 19-30.
- (21) Chuayjujit, S.; Sakulkijpiboon, S.; Potiyaraj, P. Preparation of Thermoplastic Elastomer from Epoxidised Natural Rubber and Polystyrene. Polym. Polym. Compos. 2010, 18, 139.
- (22) Kuo, S. W.; Lin, C. L.; Chang, F. C. The Study of Hydrogen Bonding and Miscibility in Poly(vinylpyridines) with Phenolic Resin. Polymer 2002, 43, 3943.
- (23) Kwak, J.; Han, S. H.; Moon, H. C.; Kim, J. K.; Koo, J.; Lee, J. S.; Pryamitsyn, V.; Ganesan, V. Phase Behavior of Binary Blend Consisting of Asymmetric Polystyrene-block-Poly(2-Vinylpyridine) Copolymer and Asymmetric Deuterated Polystyrene-block-Poly(4-Hydroxystyrene) Copolymer. Macromolecules 2015, 48, 1262.
- (24) Patyukova, E.; Rottreau, T.; Evans, R.; Topham, P. D.; Greenall, M. J. Hydrogen Bonding Aggregation in Acrylamide: Theory and Experiment. Macromolecules 2018, 51, 7032.
- (25) Kim, S. O.; Solak, H. H.; Stoykovich, M. P.; Ferrier, N. J.; de Pablo, J. J.; Nealey, P. F. Epitaxial Self-Assembly of Block Copolymers on Lithographically Defined Nanopatterned Substrates. Nature 2003, 424, 411.
- (26) Stoykovich, M. P.; Müller, M.; Kim, S. O.; Solak, H. H.; Edwards, E. W.; de Pablo, J. J.; Nealey, P. F. Directed Assembly of Block Copolymer Blends into Nonregular Device-Oriented Structures. Science 2005, 308, 1442.
- (27) Wan, L.; Ruiz, R.; Gao, H.; Patel, K. C.; Albrecht, T. R.; Yin, J.; Kim, J.; Cao, Y.; Lin, G. The Limits of Lamellae-Forming PS-b-PMMA Block Copolymers for Lithography. ACS Nano 2015, 9, 7506.
- (28) Zhou, S. X.; Janes, D. W.; Kim, C. B.; Willson, C. G.; Ellison, C. J. Designing Intrablock Attractions To Increase the χ Parameter of a Symmetric Diblock Copolymer. Macromolecules 2016, 49, 8332.
- (29) Seshimo, T.; Maeda, R.; Odashima, R.; Takenaka, Y.; Kawana, D.; Ohmori, K.; Hayakawa, T. Perpendicularly Oriented Sub-10-nm Block Copolymer Lamellae by Atmospheric Thermal Annealing for One Minute. Sci. Rep. 2016, 6, 19481.
- (30) Yoshimura, Y.; Chandra, A.; Nabae, Y.; Hayakawa, T. Chemically Tailored High-Chi Block Copolymers for Perpendicular Lamellae via Thermal Annealing. Soft Matter 2019, 15, 3497-3506.
- (31) Yoshida, K.; Tian, L.; Miyagi, K.; Yamazaki, A.; Mamiya, H.; Yamamoto, T.; Tajima, K.; Isono, T.; Satoh, T. Facile and Efficient Modification of Polystyrene-block-poly(methyl methacrylate) for Achieving Sub-10 nm Feature Size. Macromolecules 2018, 51, 8064.
- (32) Dehmel, R.; Dolan, J. A.; Gu, Y. B.; Wiesner, U.; Wilkinson, T. D.; Baumberg, J. J.; Steiner, U.; Wilts, B. D.; Gunkel, I. Optical Imaging of Large Gyroid Grains in Block Copolymer Templates by Confined Crystallization. Macromolecules 2017, 50, 6255-6262.
- (33) Yan, L.; Rank, C.; Mecking, S.; Winey, K. I. Gyroid and Other Ordered Morphologies in Single-Ion Conducting Polymers and Their Impact on Ion Conductivity. J. Am. Chem. Soc. 2020, 142, 857.
- (34) Hamley, I. W.; Castelletto, V., Small-Angle Scattering of Block Copolymers. In Soft-Matter Characterization, Borsali, R.; Pecora, R., Eds.; Springer: Netherlands, 2008, 1021.

- (35) Matsen, M. W.; Bates, F. S. Unifying Weak- and Strong-Segregation Block Copolymer Theories. Macromolecules 1996, 29,
- (36) Bates, F. S.; Fredrickson, G. H. Block Copolymers Designer Soft Materials. Phys. Today 1999, 52, 32.
- (37) Winey, K. I.; Gobran, D. A.; Xu, Z.; Fetters, L. J.; Thomas, E. L. Compositional Dependence of the Order-Disorder Transition in Diblock Copolymers. Macromolecules 1994, 27, 2392.
- (38) Khandpur, A. K.; Foerster, S.; Bates, F. S.; Hamley, I. W.; Ryan, A. J.; Bras, W.; Almdal, K.; Mortensen, K. Polyisoprene-Polystyrene Diblock Copolymer Phase Diagram near the Order-Disorder Transition. Macromolecules 1995, 28, 8796.
- (39) Sakurai, S.; Kawada, H.; Hashimoto, T.; Fetters, L. J. Thermoreversible Morphology Transition between Spherical and Cylindrical Microdomains of Block Copolymers. Macromolecules 1993, 26, 5796.
- (40) Wei, X. Y.; Strzalka, J. W.; Li, L.; Russell, T. P. Tailoring Block Copolymer Morphologies via Alkyne/Azide Cycloaddition. J. Polym. Sci., Part B: Polym. Phys. 2012, 50, 55-64.

□ Recommended by ACS

Synthesis and Characterization of Copolymers from Diallyldimethylammonium Hexafluorophosphate and Methyl Methacrylate

Alison R. Biery and Daniel M. Knauss

FEBRUARY 07, 2023 MACROMOLECULES

RFAD 🗹

Molecular Design of Hydrophilized Polyethersulfone to **Enhance Water/Salt Selectivity**

Chenchen Zhang, Jianqiang Meng, et al.

FEBRUARY 22, 2023

MACROMOLECULES

READ **C**

Structure and Phase Behavior of Bottlebrush Diblock **Copolymer-Linear Homopolymer Ternary Blends**

Bo Zhang, Frank S. Bates, et al.

FEBRUARY 08, 2023

MACROMOLECULES

RFAD 17

Topologically Induced Heterogeneity in Gradient Copolymer Brush Particle Materials

Yuqi Zhao, Michael R. Bockstaller, et al.

JULY 28, 2022

MACROMOLECULES

READ **C**

Get More Suggestions >